Confined Flow over Semi-circular Cylinder in Steady Flow Regime

A Dissertation Report Submitted

in partial fulfillment of the requirement for

the award of degree of

MASTERS OF TECHNOLOGY

IN

CHEMICAL ENGINEERING

Submitted by

Manish Dhiman

Roll No: 601111010

Under the Guidance of

Dr. Raj Kumar Gupta — **(Associate Professor)**

Dr. Avinash Chandra — **(Assistant Professor)**

Department of Chemical Engineering

Thapar University, Patiala.

DEPARTMENT OF CHEMICAL ENGINERING

THAPAR UNIVERSITY

PATIALA-147004, INDIA

(June 2013)

CERTIFICATE

This is to certify that the dissertation entitled "***Confined Flow over Semi-circular Cylinder in Steady Flow Regime***" is an authentic record of my own work carried out as per requirements for the award of degree of **M.Tech. (Chemical Engineering) at Thapar university, Patiala,** under the guidance of **Dr. Raj Kumar Gupta,** Associate Professor and **Dr. Avinash Chandra,** Assistant Professor, Department of Chemical Engineering, Thapar University, Patiala, during July 2012 to June 2013.

Date: 27/6/2013

Manish Dhiman
(Roll no: 601111010)

It is certified that the above statement made by the student is correct to the best of my knowledge and belief.

(Dr. Raj Kumar Gupta)
Associate Professor and PG coordinator
Department of Chemical Engineering
Thapar University
Patiala- 147004, India

(Dr. Avinash Chandra)
Assistant Professor
Department of Chemical Engineering
Thapar University
Patiala- 147004, India

Counter signed by

(Dr. Rajeev Mehta)
Associate Professor and Head
Department of Chemical Engineering
Thapar University
Patiala- 147004, India

(Dr. S. K. Mohapatra)
Dean of Academic Affairs
Thapar University
Patiala-147004, India

ACKNOWLEDGEMENT

No volume of words is enough to express my gratitude towards my guide, **Dr. Raj Kumar Gupta** (Associate Professor and PG coordinator) and **Dr. Avinash Chandra** (Assistant Professor), Department of Chemical Engineering, Thapar University, who have been very concerned and have aided for all the material essential for the preparation of this thesis report. They helped me to explore this vast topic in an organized manner and provided me with all the ideas on how to work towards a research-oriented venture.

I am also thankful to **Dr. Rajeev Mehta**, Head of Department, CHED and the faculty of the department of chemical engineering for the motivation and inspiration that triggered me for the thesis work.

I am also thankful to **Alpana Saini**, **Amit Kumar Ojha, Divyanshu Arya, Gurpreet Thandi, Parul, Rashmi Pahwa and Vikas Vats** and all other friends who were always there in the need of the hour and provided with all the help and facilities, which I required, for the completion of my thesis.

Most importantly, I would like to thank my parents and the Almighty for showing me the right direction out of the blue, to help me stay calm in the oddest of the times.

Manish Dhiman

(Roll No: 601111010)

ABSTRACT

The detailed flow and thermal fields have been presented for the steady mixed convection heat transfer from a semi-circular cylinder placed in a rectangular channel. The semi-circular cylinder is symmetrically placed in a rectangular channel in such a manner as curved surface of the semi-circular cylinder is facing the upward oncoming flow and gravity is acting in downward direction (*'-'ve y*-direction). Hence, the buoyancy is also directed in the same direction. This study spans the following ranges of conditions $1 \leq Re \leq 50$; $0.7 \leq Pr \leq 50$; $0 \leq Pr \leq 2$ and Confinement ratio (β) = 4. The numerical predictions are analyzed in terms of the distribution of pressure coefficients, drag coefficients, local and averaged Nusselt numbers over the aforementioned ranges of the influencing parameters. The streamline patterns show that the wake is being suppressed under confinement and isotherms are get clustered around semi-circular cylinder. At low Reynolds number, the maximum value of pressure coefficient found at front stagnation point followed by sudden drop at sharp corners whereas at high value of Reynolds number, the drop in the value of pressure coefficient at corners are relatively small than low Reynolds number. The maximum value of the local Nusselt number is found at front stagnation point. At the sharp corners, the local Nusselt number suddenly decreases and small recovery is seen at rear flat surface. As expected, the drag coefficient decreases with increases in the value of Reynolds number whereas the average value of Nusselt number increases with gradual increase in the value of Reynolds and Prandtl number. The Richardson number shows complex influence on the flow and heat transfer characteristics.

Table of Contents

Topic	Page No.
Certificate	i
Acknowledgement	ii
Abstract	iii
Table of Contents	iv
List of Figures	vi
List of Tables	vii
Nomenclature	viii
CHAPTER-1 INTRODUCTION	**1**
CHAPTER-2 LITERATURE REVIEW	**3**
2.1 Gap in literature	9
2.2 Objectives of the present work	9
CHAPTER -3 MATHEMATICAL FORMULATION AND NUMERICAL METHODOLOGY	**10**
3.1 Problem statement	10
3.2 Assumptions	10
3.3 Governing equations	11
3.4 Boundary conditions	11
3.5 Non dimensional parameters and equations	12
3.6 Non dimensional boundary conditions	14
3.7 Calculations of global parameters	15
3.8 Numerical methodology	16
CHAPTER -4 CHOICE OF NUMERICAL PARAMETERS	**17**
4.1 Entrance and exit length of the channel	17

4.2 Grid resolution study 19

CHAPTER -5 GENERAL VALIDATIONS 21

5.1 2-D Lid-driven cavity flow 21

5.2 Steady flow over semi-circular cylinder 23

5.3 Forced convection heat transfer over horizontal circular cylinder within confining wall in a rectangular channel 25

CHAPTER -6 RESULTS AND DISCUSSION 27

6.1 Fluid flow characteristics 27

6.1.1 Streamline patterns 27

6.1.2 Pressure coefficients 30

6.1.3 Drag coefficients 30

6.2 Heat transfer 33

6.2.1 Isotherm patterns 33

6.2.2 Local Nusselt number 33

6.2.3 Average Nusselt number 33

CHAPTER -7 CONCLUSIONS AND FUTURE RECOMMENDATIONS 37

REFERENCES 38

List of figures

Figure **Page No.**

Chapter -3

3.1 Schematic presentation of computational domain 13

3.2 Schematic presentation of the physical model 13

Chapter -5

5.1 Schematics of lid-driven cavity flow 21

5.2 Comparison of centerline U_X velocity 22

5.3 Comparison of centerline U_Y velocity 22

5.4 Schematic presentation of the semi-circular cylinder 24

5.5 Schematic presentation of the circular cylinder within confined wall 26

Chapter -6

6.1 Streamline patterns and isotherms at Pr=0.7 28

6.2 Streamline patterns and isotherms at Pr=50 29

6.3 Distribution of pressure coefficient along the surface of semi-circular cylinder 31

6.4 Distribution of drag coefficient along the surface of semi-circular cylinder 32

6.5 Distribution of Nusselt number along the surface of semi-circular cylinder 34

6.6 Distribution of average Nusselt number along the surface of semi-circular cylinder 35

6.7 Distribution of average Nusselt number along the surface of semi-circular cylinder 36

List of tables

Table	Page No.
Chapter -2	
2.1 Literature reviews for single and multiple circular cylinders	3
2.2 Literature reviews for confined non-circular cylinders	4
2.3 Literature reviews for semi-circular cylinders	5
Chapter -4	
4.1 Entrance length (L_{in}) independence	17
4.2 Exit length (L_{out}) independence	18
4.3 Grid details	19
4.4 Grid independence study	20
Chapter -5	
5.1 Comparison of drag coefficients at different Reynolds number value	24
5.2 Comparison of results	26
Chapter -6	
6.1 Dependence of C_D on *Re*, *Ri* and *Pr*	36

Nomenclature

c	Specific heat of the fluid (J/kg.K)
C_D	Total drag coefficient (dimensionless)
C_{DF}	Friction drag coefficient (dimensionless)
C_{DP}	Pressure drag coefficient (dimensionless)
C_L	Lift coefficient (dimensionless)
C_P	Pressure coefficient (dimensionless)
D	Diameter of cylinder (m)
D_∞	Diameter of computational domain (m)
F_D	Total drag force per unit length of the cylinder (N/m)
F_{DF}	Friction drag force per unit length of the cylinder (N/m)
F_{DP}	Pressure drag force per unit length of the cylinder (N/m)
g	Acceleration due to gravity
G1, G2, G3	Grid labels
Gr	Grashof number (dimensionless)
h	Heat transfer coefficient (W/ m^2 k)
k	Thermal conductivity of fluid (W/ m k)
L_{in}	Entrance Length (m)
L_{out}	Exit length (m)
N	Total number of cells (dimensionless)
N_P	Number of points at cylinder surface (dimensionless)
Nu	Local Nusselt number (dimensionless)
Nu_{avg}	Average Nusselt number (dimensionless)
P	Pressure (Pa)
P_S	Local surface pressure (Pa)

P_∞	Free stream pressure (Pa)
Pr	Prandtl number (dimensionless)
Ra	Rayleigh number (dimensionless)
Re	Reynolds number (dimensionless)
Ri	Richardson number (dimensionless)
S	Surface area (m^2)
T	Fluid temperature (K)
T_W	Wall temperature at the surface of the semi-circular cylinder (K)
T_∞	Fluid temperature at inlet (K)
U	Velocity (m/s^2)
U_x	x-component velocity (m/s^2)
U_y	y-component velocity (m/s^2)
U_∞	Free stream velocity at inlet (m/s^2)

Greek symbols

β	Confinement ratio
β_v	Coefficient of volumetric thermal expansion (1/K)
δ	Grid spacing in the vicinity of the cylinder (m)
ρ	Density of the fluid (kg/m^3)
Φ	Dependent variables like U_x, U_y and T
μ	Dynamic viscosity of the fluid (Pa.s)

Subscripts

i, j, x, y	Cartesian coordinates

Superscripts

’	Dimensional variable

CHAPTER - 1

Introduction

Flow around bluff bodies has been a topic of research for last several years due to its engineering and theoretical importance. It constitutes an important class of fundamental problem in the domain of fluid mechanics and heat transfer.

These studies provides useful insights into the nature of underlying physical phenomena such as drag coefficients, lift coefficients, wake characteristics, isotherm, local distribution of Nusselt number and average Nusselt number etc. The flow and heat transfer characteristics are the functions of the field variables (*Re, Pr, Ri, Nu* and Nu_{avg}), body geometry and degree of confinements. Such model flow configurations represent the idealization of many real problems and processes encountered in nature and in technology as well. Thus reliable comparative data on the different structures are valuable for technological development or to understand the existing flow and heat transfer phenomenon. There are many industrial applications for the present flow configuration and heat transfer and it serves as model configuration, e.g. cooling towers, chimney, compact heat exchangers, cooling components, and many more. Specifically, recent engineering and industrial applications are frequently using noncircular tubes in heat transfer applications. Semicircular cylinder is of particular interest for chemical and food industries (e.g. thermal processing of sliced carrot along their long axis), solar engineering applications, flow over semi-circular tubes in novel heat exchangers, electronic cooling and some of the submarines with their flat base can be visualized in terms of the flow over a semicircular cylinder. Additional applications are found in polymer processing operations where the most of the fluids exhibit non Newtonian behavior and variously shaped objects are used as flow dividers.

The flow and heat transfer characteristics are influenced by large number of factors such as the number of obstacles, cross sectional shape and orientation of the bluff body, the nature of approaching flow (laminar or turbulent) and the type of the fluid (compressible or incompressible), nature of confinement, operating range of Reynolds number and angle of incidence, etc.

The bluff body includes cylinder of various cross-sections such as circular, square, elliptical, triangle, semi-circular etc. The flow and heat transfer fields are greatly influenced by the cross-sectional shape of the cylinder.

For instance, in case of semi-circular cylinder, the flow behavior depends upon on the orientation of the cylinder to the direction of the flow, for the case of curved surface facing the flow directions, the flow get separated at *Re* 15 and the steady flow regime end up at *Re* = 30. (*Chandra and Chhabra*, 2011). It also influenced by the type of the operating fluid (shear thinning, shear thickening, viscous, Newtonian and non-Newtonian flow). For instance, in case of heat transfer from an unconfined semi-circular cylinder, the maximum heat transfer occurs at the front surface of the cylinder and the sharp corners, while, rear flat surface contributes less. Furthermore, this behavior changes with the range of Reynolds number, Richardson number, Prandtl number, Nusselt number and average Nusselt number. In comparison with circular cylinder, semi-circular cylinder is having the geometrical complexity and asymmetric. Hence, flow and heat transfer characteristics are quite different in nature for semi-circular cylinder.

In this, study we are aiming to explore the influence of channel wall on the flow and heat transfer characteristics from a semi-circular cylinder. A semi-circular cylinder is kept in a channel of confinement $\beta=4$.

CHAPTER – 2

Literature review

This chapter presents a review of the previous work related to the flow and heat transfer across various shapes of cylinder like circular or square cylinders etc. The fluid flow and heat transfer from a cylinder immersed in streaming fluid is influenced by large number of variables such as body shape, confinement, blockage ratio, *Re*, *Pr* etc.

Table: 2.1: *Literature reviews for single and multiple circular cylinders*

Source	Range of conditions	Remarks
Sanitjai and Goldstein (2004)	Experimental, Forced convection, $2\times10^{3} \leq Re \leq 10^{5}$, $.7 \leq Pr \leq 180$	Detailed streamline and isotherm profile were presented. The *Nu* at the front stagnation point $Nu = f(Re^{0.5}, Pr^{.3})$.
Soars et al. (2005)	Numerical, Forced convection, $5 \leq Re \leq 40$, $1 \leq Pr \leq 100$, $0.5 \leq n \leq 1.4$	The maximum value of *Nu* was found at the front stagnation point. The drag value increased with increase in *Re* and *n*. The CHF provided more heat transfer than CWT.
Soars et al. (2009)	Numerical, Mixed convection, $0 \leq Ri \leq 3$, $1 \leq Re \leq 30$, $1 \leq Pr \leq 100$, $0.6 \leq n \leq 1.6$	Nu_{avg} increased with *Pr, Re* and *Ri*. The influence of *Ri* increased with *n*. C_D decreased with *Re* and *n*.
Salleh et al. (2010)	Numerical, Mixed convection, $1 \leq Re \leq 40$, $0.72 \leq Pr \leq 100$, $0.5 \leq \beta \leq 1.9$.	The influence of confinement has been shown. The boundary layer separation point moved towards rear stagnation point with increase in β and vice-versa.

Table: 2.2: *Literature reviews for confined non-circular cylinders*

Source	Range of conditions	Remarks
Abbasai et al.(2002)	Numerical, Steady forced convection, Triangular prism, $30 \leq Re \leq 200$, $Pr = 0.71$, $0 \leq Gr \leq 1.5 \times 10^4$	Stanton number and Nu_{avg} were function of *Re*. The influence of vortex shedding has been shown.
Cruchaga and Celentano (2002)	Numerical, Steady mixed convection, Square cylinder, $100 \leq Re \leq 500$, $0 \leq Gr \leq 32 \times 10^4$	The influence of *Gr* on friction coefficients along the wall has been studied. It is shown that temperature distributions were strongly affected by the buoyancy
Dhiman et al.(2007)	Numerical, Steady mixed convection, Square cylinder, $0 \leq Ri \leq 1$, $1 \leq Re \leq 30$, $7 \leq Pr \leq 100$, $\beta = 0.125$.	*Ri* having more influence on C_L than C_D. The degree of asymmetry increased with the value of the *Ri* increase from 0 to 1.
Dhiman et al.(2007)	Numerical, Steady mixed convection, Square cylinder, $0 \leq Ri \leq 0.5$, $1 \leq Re \leq 30$, $0.7 \leq Pr \leq 100$, $0.8 \leq n \leq 1.5$.	The influence of *Ri* on *Nu* has been presented.
Sahu et al. (2009)	Numerical, Unsteady forced convection, Square cylinder, $60 \leq Re \leq 160$, $0.7 \leq Pr \leq 50$, $0.5 \leq n \leq 1.4$.	Nu increased with *Re* and *Pr*. The heat transfer from front half was found more than rear half of the cylinder.
Chatterjee and Amiroudine (2009)	Numerical, Steady mixed convection, Square cylinder, $0 \leq Ri \leq 1$,$1 \leq Re \leq 30$, $0.7 \leq Pr \leq 100$, $\beta =$ 0.10 %	The drag coefficients shown complex dependencies on *Ri*.

Chhabra et al.(2007)	Numerical, Steady forced convection, Elliptical cylinder. $01 \leq Re \leq 40$, $1 \leq Pr \leq 100$, $0.2 \leq n \leq 1.8$, $0.2 \leq E \leq 5$.	Nu = f (Re, n, Pr, and E). The Nu_{avg} increased with Pr and Re. Heat transfer increased with increase in the value of the n.
Patil et al. (2008)	Numerical, Steady forced convection, Circular cylinder, $.01 \leq Re \leq 40$, $1 \leq Pr \leq 100$, $0.2 \leq n \leq 1.8$, $2 \leq \beta \leq 10$.	The Nu_{avg} increased with Re, Pr and n. Heat transfer decreased with increase in the value of the n.
Srinivas et al.(2009)	Numerical, Steady mixed convection, Horizontal circular cylinder, $0 \leq Ri \leq 2$, $1 \leq Re \leq 40$, $1 \leq Pr \leq 100$, $0.2 \leq n \leq 1.8$	The C_P decreased with increase in Re and Pr. The rate of heat transfer increased with Re, Ri, and Pr and decreased with n.
Ishak (2009)	Numerical, Steady mixed convection, Vertical circular cylinder, $0.7 \leq Pr \leq 10$.	The boundary layer separation was delayed for a cylinder as compared to a flat plate.
Dhole et al. (2006)	Numerical, Steady forced convection, Sphere cylinder, $5 \leq Re \leq 200$, $1 \leq Pr \leq 400$, $0.5 \leq n \leq 2$.	The value of Nu_{avg} increases with Re, Pr and it decrease with increasing value of n.

Table: 2.3: *Literature reviews for semi-circular cylinders*

Source	Range of conditions	Remarks
Kiya et al. (1975)	Numerical study, 2-D, semi-circular and semi-elliptical projection, Navier-Stokes equations, $60 \leq Re \leq 100$.	The Re was a function of geometrical shape of the front and rear vortices, drag coefficients and distribution of pressure and shear stress.
Karniadakis and Brown (1995)	Numerical study, Re=150.	The 2-D and 3-D simulations were carried out. They examined the $3-D$ influences the flow structure for an unsteady shear flow.

Kumarasay and Barlow (1995)	Experimental study, Re=4.67×10^5.	The pressure distribution of unsteady pressure at separation points was reported. The vortex shedding vanished at the critical gap ratio of 0.33 times the diameter of the cylinder.
Boisaubert et al. (1996)	Experimental study, 60≤Re≤100, β=0.14	The flow was visualized showing the comparative wakes and flow fields for two opposite arrangements. (curved face and flat face)
Boisaubert et al. (1997)	Experimental study, Re=100	The flow field has been visualized by using dispersed solid particles and dye filaments. The initial formation and shedding of the vortices behind a semi-circular cylinder has been reported.
Boisaubert and Texier, (1998)	Experimental study, 60≤Re≤100.	The effect of gap between the semi-circular and the splitter plate on the wake was obtained. The wake length increased with increasing in the value of Re.
Coutanceau et al. (2000)	Experimental study, 60≤Re≤200.	The flow field has been visualized by using dispersed solid particles and dye filaments. The wake was mostly affected by back concave wall of the shell.
Sophy et al. (2002)	Numerical study, Re=65.	The laminar periodic regime has been observed at Re=65.

Nada et al. (2003)	Experimental study, Free convection, $10^9 \leq Re \leq 6\times10^{9.}$	The convective heat transfer coefficient was found as a function of the Rayleigh number, inclination angle, and orientation angle of the semi-circular cylinder. The *Nu* increased with the angle of inclination.
Nada et al. (2007)	Experimental and numerical study, $2.2\times10^3 \leq Re \leq 4.5\times10^{9.}$	The Nu_{avg} increased the angle of attack. The Nu_{avg} increased with increase in Reynolds number
Hocking et al. (2008)	Numerical study, 0 ≤Froude number ≤5.	The results were presented to show the influence of gravity on wake size for the flow over a semi-circular cylinder. They found narrow and long wake region for the upward facing curved surface configuration and wide and short wake region for the downward facing curved surface configuration
Chandra and Chhabra (2011)	Numerical, Steady mixed convection, $0 \leq Ri \leq 2$, $1 \leq Re \leq 30$, $1 \leq Pr \leq 100$, $0.2 \leq n \leq 6$.	At *Re*=1, *Nu* was found to be maximum at corners and for high *Re*, it shifted towards the front stagnation point. The Nu_{avg} increased with *Re*, *Pr* and *Ri*.
Chandra and Chhabra (2011)	Numerical, Steady forced convection, $0.01 \leq Re \leq 30$, $1 \leq Pr \leq 100$, $0.2 \leq n \leq 1.8$.	The C_D decreased with increase in *Re*, for $n<1$ at low *Re*. The Nu_{avg} increased with *Re*, *Pr* and *Ri*. Heat transfer increased with the higher value of power law index.

Chandra and Chhabra (2012)	Numerically, Free convection, $10 \leq Gr \leq 10^5$, $0.72 \leq Pr \leq 100$, $0.2 \leq n \leq 1.8$.	The Nu_{avg} increased with *Gr* and *Pr.* The flow remain attached to the surface of the semi-circular cylinder for $n>1$.

2.1 Gap in literature

Based on the detailed discussion on the available literature, it is thus fair to conclude that no study is available on mixed convection heat transfer characteristics from a semi-circular cylinder placed in rectangular channel. The present work aims to fill this gap in literature by exploring the mixed convection heat transfer from a confined semi-circular cylinder in the steady flow regime.

2.2 Objectives of the present work

The following objectives have been set for the present study on the mixed convection (aiding buoyancy) heat transfer from heated semi-circular cylinder placed in a rectangular channel.

(a) To study the influence of channel confinement of $\beta = 4$ on flow and heat transfer characteristics under gravity.

(b) To study the influence of Richardson number (*Ri*), Reynolds number (*Re*) and Prandtl number (*Pr*).

CHAPTER – 3

Mathematical formulation and numerical methodology

This chapter represents the mathematical equations describing the confined mixed convection heat transfer from semi-circular cylinder together with the relevant boundary conditions. The equations to calculate the individual and total drag coefficient, Nusselt number and stream function and isotherm patterns are represented in this chapter.

3.1 Problem statement

The two-dimensional laminar flow of incompressible fluid against gravity (aiding buoyancy) with a uniform velocity U_∞ and temperature of T_∞ over a semi-circular cylinder under confinement ratio (β=4) shown in fig 3.1.The surface of the semi-circular cylinder is maintained at a constant wall temperature $T_{w.}$ The diameter of semi-circular cylinder is D. The semi-circular cylinder is placed at an upstream distance L_{in} from the inlet with a downstream distance L_{out}. The value of L_{in} is chosen sufficiently large in order to get fully developed velocity profile before the semi-circular cylinder.

3.2 Assumptions

The complication arises due to the coupling of the momentum and energy equation in the case of mixed convection heat transfer with gravity term. Therefore, in order to keep the level of complexity at a lower level, the following assumptions are made for the present investigation.

Incompressible fluid.

2D, laminar flow.

Infinite long semicircular cylinder in z-direction

No viscous dissipation.

The Boussinesq approximation is used for the body force term.

Constant physico-chemical properties of the fluid other than density.

3.3 Governing equations

The governing differential equations used here are the mass and momentum equations in their dimensional form.

Continuity Equation:

$$\frac{\partial(U_x^{'})}{\partial x^{'}} + \frac{\partial\left(U_y^{'}\right)}{\partial y^{'}} = 0 \tag{1}$$

Equation of motion:

$$\rho\left(\frac{\partial(U_x^{'}U_x^{'})}{\partial x^{'}} + \frac{\partial(U_y^{'}U_x^{'})}{\partial y^{'}}\right) = -\frac{\partial P^{'}}{\partial x^{'}} + \mu\left(\frac{\partial^2 U_x^{'}}{\partial x^{'2}} + \frac{\partial^2 U_x^{'}}{\partial y^{'2}}\right) \tag{2}$$

$$\rho\left(\frac{\partial(U_x^{'}U_y^{'})}{\partial x^{'}} + \frac{\partial(U_y^{'}U_y^{'})}{\partial y^{'}}\right) = -\frac{\partial P^{'}}{\partial y^{'}} + \mu\left(\frac{\partial^2 U_y^{'}}{\partial x^{'2}} + \frac{\partial^2 U_y^{'}}{\partial y^{'2}}\right) + g_y\rho \tag{3}$$

Energy equation:

$$\rho C_p\left(\frac{\partial(U_x^{'}T^{'})}{\partial x^{'}} + \frac{\partial(U_y^{'}T^{'})}{\partial y^{'}}\right) = k\left(\frac{\partial^2 T^{'}}{\partial x^{'2}} + \frac{\partial^2 T^{'}}{\partial y^{'2}}\right) \tag{4}$$

Boussinesg approximation

$$\rho = \rho_\infty\,[1 - \beta(T - T_\infty)] \tag{5}$$

3.4 Boundary conditions

The boundary conditions for this flow are given as follow.

Inlet boundary: Uniform flow and temperature condition, i.e.

$$U_x^{'} = 0 \;\; ; \;\; U_y^{'} = U_\infty \;\; ; \;\; T^{'} = T_\infty. \tag{6}$$

No-slip boundary condition at the surface of the semi-circular cylinder and at the confined wall flow is imposed.

$$U_x^{'} = 0 \;\; ; \;\; U_y^{'} = 0 \;\; ; \;\; T^{'} = T_w. \tag{7}$$

At channel wall:

$$U_x^{'} = 0 \;\; ; \;\; U_y^{'} = 0 \;\; ; \;\; q^{'} = 0 \tag{8}$$

Outlet boundary:

The outflow boundary condition in FLUENT is defined as

$$\frac{\partial \emptyset}{\partial y} = 0 \tag{9}$$

where $\emptyset = U_x^{'}, U_y^{'}$ and $T^{'}$.

3.5 Non-dimensional parameters and equations

- Length D
- Velocity U_∞
- Pressure $\rho U^2{}_\infty$
- Temperature $T = (T' — T_\infty) / (T_w — T_\infty)$

Reynolds number:

$$Re = \frac{\rho D U_y}{\mu} \tag{10}$$

Grashof number:

$$Gr = \frac{g\, \rho^2\ \beta D^3\ (T_w - T_\infty)}{\mu^2} \tag{11}$$

Prandtl number:

$$Pr = \frac{\mu\, c_p}{k} \tag{12}$$

Richardson number:

$$Ri = \frac{Gr}{Re^2} \tag{13}$$

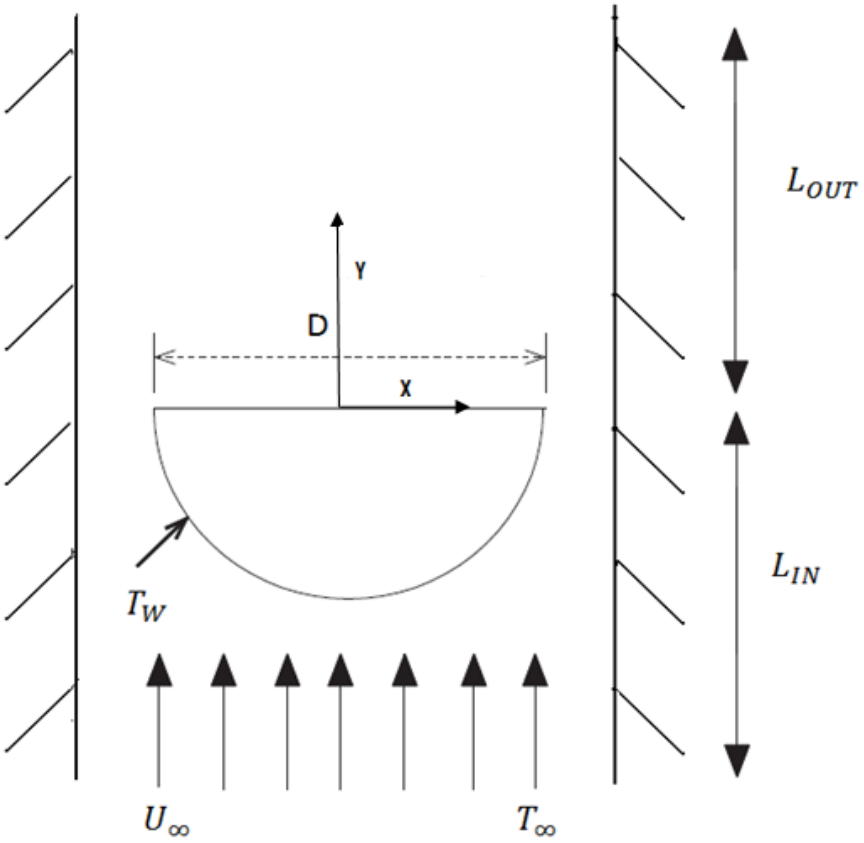

Fig 3.1: *Schematic presentation of the computational domain*

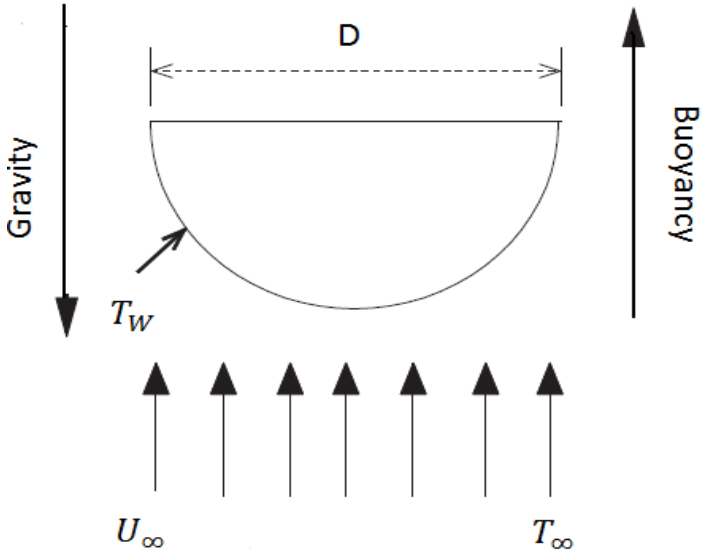

Fig 3.2: *Schematic presentation of the physical model*

The governing equations in their non-dimensional forms are written as follows.

Continuity Equation:

$$\frac{\partial(U_x)}{\partial x} + \frac{\partial\left(U_y\right)}{\partial y} = 0 \tag{14}$$

Equation of motion:

$$\frac{\partial(U_x U_x)}{\partial x} + \frac{\partial(U_y U_x)}{\partial y} = -\frac{\partial P}{\partial x} + \frac{1}{Re}\left(\frac{\partial^2 U_x}{\partial x^2} + \frac{\partial^2 U_x}{\partial y^2}\right) \tag{15}$$

$$\frac{\partial(U_x U_y)}{\partial x} + \frac{\partial(U_y U_y)}{\partial y} = -\frac{\partial P}{\partial y} + \frac{1}{Re}\left(\frac{\partial^2 U_y}{\partial x^2} + \frac{\partial^2 U_y}{\partial y^2}\right) + R_i T \tag{16}$$

Energy equation:

$$\frac{\partial(U_x T)}{\partial x} + \frac{\partial(U_y T)}{\partial y} = \frac{1}{Re.Pr}\left(\frac{\partial^2 T}{\partial x^2} + \frac{\partial^2 T}{\partial y^2}\right) \tag{17}$$

3.6 Non-dimensional boundary conditions

The boundary conditions can also be non-dimensionalized and presented as follow:

Inlet boundary:

$$U_x = 0 \;\; ; \;\; U_y = 1 \; ; \;\; T = 0 \tag{18}$$

No-slip boundary condition at the surface of the semi-circular cylinder:

$$U_x = 0 \;\; ; \;\; U_y = 0 \; ; \;\; T = 1 \tag{19}$$

At channel wall:

$$U_x = 0 \;\; ; \;\; U_y = 0 \; ; \;\; q = 0 \tag{20}$$

Outlet boundary conditions:

$$\frac{\partial \emptyset}{\partial y} = 0 \tag{21}$$

where $\emptyset = U_x,\ U_y$ and T.

3.7 Calculation of global parameters

Pressure coefficient:

The ratio of the static pressure to the dynamic pressure on the surface of the semi-cylinder is called the pressure coefficient given as follow.

$$C_P = \frac{P_s - P_\infty}{\frac{1}{2}\rho U_\infty} \tag{22}$$

Drag coefficients:

The total drag forces draw contributions from the friction and pressure forces and these forces are presented in the form of the dimensionless friction and pressure drag coefficients. The total drag coefficient is the sum of these two types of drag.

C_D is called total drag coefficient and is the sum of $C_{DP} + C_{DF}$.

$$C_D = \frac{F_D}{\frac{1}{2}\rho U_\infty^2 D} \tag{23}$$

$$C_{DP} = \frac{F_{DP}}{\frac{1}{2}\rho U_\infty^2 D} \tag{24}$$

$$C_{DF} = \frac{F_{DF}}{\frac{1}{2}\rho U_\infty^2 D} \tag{25}$$

C_{DP} represents the pressure drag and C_{DF} represents the friction drags

Nusselt number:

The rate of heat transfer from the cylinder to fluid and from the fluid to cylinder is represented by the Nusselt number, *Nu*.

$$N_u = \frac{hD}{K} \tag{26}$$

3.8 Numerical methodology

The governing partial differential equations of the flow and heat transfer for the flow over a semi-circular cylinder with appropriate boundary conditions were solved numerically using the ANSYS FLUENT (version 6.3.26) over an unstructured mesh of uniform grid spacing at the surface of semi-circular cylinder. The grid was generated in the GAMBIT (version 2.3.16). In order to capture the steep gradients near the surface of the semi-circular cylinder, sufficiently fine grid was chosen in the vicinity of the semi-circular cylinder. The two dimensional, steady, laminar, coupled solver was used to solve the incompressible flow on the collocated grid arrangement. The second order upwind scheme has been used to discretize the convective terms of the momentum and energy transport equations and the SIMPLE (semi-implicit method for the pressure linked equations) scheme was employed for solving the pressure-velocity coupling. The Gauss–Siedel (G–S) point-by-point iterative method in conjunction with the algebraic multi-grid (AMG) method was used to solve the system of algebraic equations. The convergence criterion of 10^{-8} was used for the residuals of the continuity and momentum equations and that of 10^{-13} for the residuals of the energy equation.

CHAPTER – 4

Choice of numerical parameters

This chapter presents the optimization choice of numerical parameters for the present work such as entrance and exit length of the channel, grid size, number of cells, convergence etc.

4.1 Entrance and exit length of the channel

The accuracy and reliability of the numerical results might be achieved by optimizing the entrance and exit length of the channel. The independence study has been done for the extreme combinations of Reynolds number 1, 50, Prandtl number 0.7, 50 and Richardson number 0, 2. The four values of L_{in} as 25, 30, 40 and 50 have been chosen. The value of the C_{DP}, C_D and Nu_{avg} have been compared and the less than 1% variation is set to be accepted. The values of C_{DP}, C_D and Nu_{avg} have been presented in Table 4.1. The observation of Table 4.1 shows that the values of C_{DP}, C_D and Nu_{avg} are almost similar for all the values of L_{in} and L_{in} = 30 has been chosen for the present work on safe hand.

Similarly, four values of L_{out} have been chosen for the optimization of exit length. The comparison of C_{DP}, C_D and Nu_{avg} are shown in Table 4.2. The data reported in Table 4.2 suggest that the L_{out} = 40 is the good choice among the four values of L_{out} = 30, 40, 50 and 60. Hence, L_{out} = 40 has been chosen as optimum value.

Table 4.1: *Entrance length (L_{in}) independence*

Pr	***Ri***	***Re***	L_{in}/D	L_{out}/D	C_{DP}	C_D	Nu_{avg}
0.7	0	1	25	50	19.65	28.24	0.8380
0.7	0	1	**30**	50	19.68	28.25	0.8380
0.7	0	1	40	50	19.61	28.22	0.8380
0.7	0	1	50	50	19.66	28.26	0.8380
0.7	2	50	25	50	2.08	2.73	5.242
0.7	2	50	**30**	50	2.09	2.74	5.2573
0.7	2	50	40	50	2.18	2.75	5.2742
0.7	2	50	50	50	2.11	2.76	5.2771
50	0	1	25	50	19.65	28.25	4.4977

50	0	1	**30**	50	19.68	28.25	4.4969
50	0	1	40	50	19.61	28.2	4.4972
50	0	1	50	50	19.66	28.26	4.4967
50	2	50	25	50	1.81	2.35	22.4821
50	2	50	**30**	50	1.82	2.36	22.4912
50	2	50	40	50	1.84	2.38	22.6867
50	2	50	50	50	1.83	2.37	22.6854
0.7	0	50	25	50	1.36	1.79	4.8858
0.7	0	50	**30**	50	1.37	1.81	4.9018
0.7	0	50	40	50	1.38	1.82	4.9195
0.7	0	50	50	50	1.38	1.83	4.9240
0.7	2	1	25	50	8.78	28.36	0.8385
0.7	2	1	**30**	50	8.75	28.37	0.8385
0.7	2	1	40	50	8.80	28.34	0.8385
0.7	2	1	50	50	8.78	28.38	0.8386

Table 4.2: *Exit length (L_{out}) independence*

Pr	***Ri***	***Re***	***L_{in}/D***	***L_{out}/D***	***C_{DP}***	***C_D***	***Nu_{avg}***
0.7	0	1	**30**	30	19.65	28.26	0.8380
0.7	0	1	**30**	**40**	19.74	28.27	0.8379
0.7	0	1	**30**	50	19.73	28.27	0.8379
0.7	0	1	**30**	60	19.72	28.27	0.8379
0.7	2	50	**30**	30	2.09	2.74	5.2572
0.7	2	50	**30**	**40**	2.09	2.74	5.2549
0.7	2	50	**30**	50	2.09	2.74	5.2544
0.7	2	50	**30**	60	2.098	2.74	5.2549
50	0	1	**30**	30	19.65	28.26	4.4983
50	0	1	**30**	**40**	19.74	28.27	4.4963
50	0	1	**30**	50	19.73	28.27	4.4968
50	0	1	**30**	60	19.72	28.27	4.4972
50	2	50	**30**	30	1.83	2.37	22.6180

50	2	50	**30**	**40**	1.82	2.36	22.4067
50	2	50	**30**	50	1.84	2.39	22.4581
50	2	50	**30**	60	1.82	2.36	22.3599
0.7	0	50	**30**	**40**	1.37	1.81	4.9001
0.7	0	50	**30**	50	1.37	1.81	4.8995
0.7	0	50	**30**	60	1.37	1.81	4.8998
0.7	2	1	**30**	30	8.78	28.38	0.8385
0.7	2	1	**30**	**40**	8.71	28.39	0.8385
0.7	2	1	**30**	50	8.72	28.39	0.8385
0.7	2	1	**30**	60	8.73	28.38	0.8384

4.2 Grid resolution study

The grid independence study has been performed on the three different grids labeled as G1, G2 and G3. The grid details are presented in Table 4.3. Again C_{DP}, C_D and Nu_{avg} has been compared and presented in Table 4.4. The observation of the Table 4.4 shows that the variation in the values of C_{DP}, C_D and Nu_{avg} is less than 2-3% for the grid G2 and G3. In addition, grid G3 is more complex than G2 and requires high computing resources and excessive computational time. Hence, the grid G2 is chosen as optimum for the entire range of the Reynolds number and it denotes the good compromise between the accuracy on one hand and the required computational effort on the other.

Table 4.3: *Grid details*

Grid label	G1	G2	G3
Spacing at cylinder surface (δ/D)	.017	.007	.005
No. of points at cylinder surface (*Np*)	72	180	260
Total no of cells (*N*)	24,120	58,940	1, 31,002

Table 4.4: *Grid independence study*

Grid label	***Pr***	***Ri***	***Re***	C_{DP}	C_{DF}	C_D	***Nu(avg)***
G1	0.7	0	1	19.74	8.53	28.27	0.8379
G2	0.7	0	1	20.07	8.40	28.47	0.8381
G3	0.7	0	1	20.19	8.34	28.53	0.8386
G1	0.7	0	50	1.374	0.43	1.81	4.9001
G2	0.7	0	50	1.37	0.43	1.81	4.8971
G3	0.7	0	50	1.38	0.44	1.82	4.8962
G1	0.7	2	1	19.68	8.71	0.83	28.3971
G2	0.7	2	1	20.02	8.57	28.60	0.8385
G3	0.7	2	1	20.14	8.51	28.65	0.8386
G1	0.7	2	50	2.09	0.64	2.74	5.2549
G2	0.7	2	50	2.11	0.63	2.75	5.2491
G3	0.7	2	50	2.12	0.63	2.75	5.2484
G1	50	0	1	19.74	8.53	28.27	4.4963
G2	50	0	1	20.07	8.41	28.47	4.4939
G3	50	0	1	20.19	8.34	28.53	4.5025
G1	50	0	50	1.36	0.43	1.81	24.3981
G2	50	0	50	1.37	0.43	1.81	23.8025
G3	50	0	50	1.38	0.43	1.81	23.2177
G2	50	2	1	20.64	8.73	4.53	29.3812
G2	50	2	1	20.98	8.59	29.58	4.5293
G3	50	2	1	21.11	8.52	29.64	4.5378
G1	50	2	50	1.82	0.54	22.40	2.3677
G2	50	2	50	1.83	0.52	2.35	21.4342
G3	50	2	50	1.84	0.52	2.37	21.7636

CHAPTER – 5

General validations

In this chapter, the series of benchmarking problems have been solved to validate the numerical methodology and process used here. The obtained results have been compared with literature values.

5.1 2-D Lid-driven cavity flow

The flow of an incompressible fluid is induced in a square cavity (of side *L*) by the motion of the top lid with a uniform velocity, U_∞ in the x-direction. The schematics of the flow are shown in fig 5.1. This problem can be considered as a basis for examining the efficiency of numerical techniques for this problem. The results are computed and compared with (*Ghia et al.*, 1982). The boundary conditions (non-dimensional) used here are as follows.

The no-slip boundary condition is used at the left, right and bottom walls.

$$U_x = 0; \qquad U_y = 0. \tag{27}$$

At the top wall

$$U_x = 1; \qquad U_y = 0. \tag{28}$$

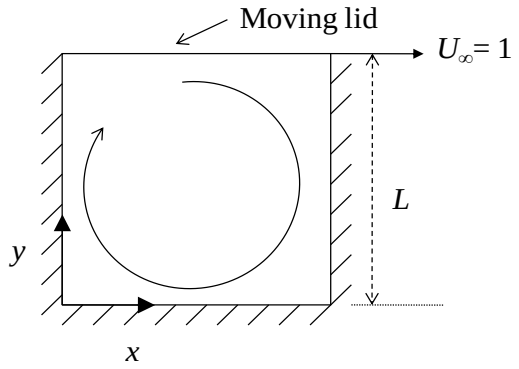

Figure 5.1: *Schematics of lid-driven cavity flow*

The present values of the *x*-velocity and *y*-velocity at the vertical and horizontal centerlines respectively of the cavity at Reynolds number, *Re* = 100, 400, 1000 are presented in figures

5.2 and 5.3. The Reynolds number for lid-driven cavity flow of is defined as $Re = \frac{\rho L U_x}{\mu}$.

The presented results show the maximum difference of ±1.47%, which shows good agreement with the results reported in literature (*Ghia et al., 1982*).

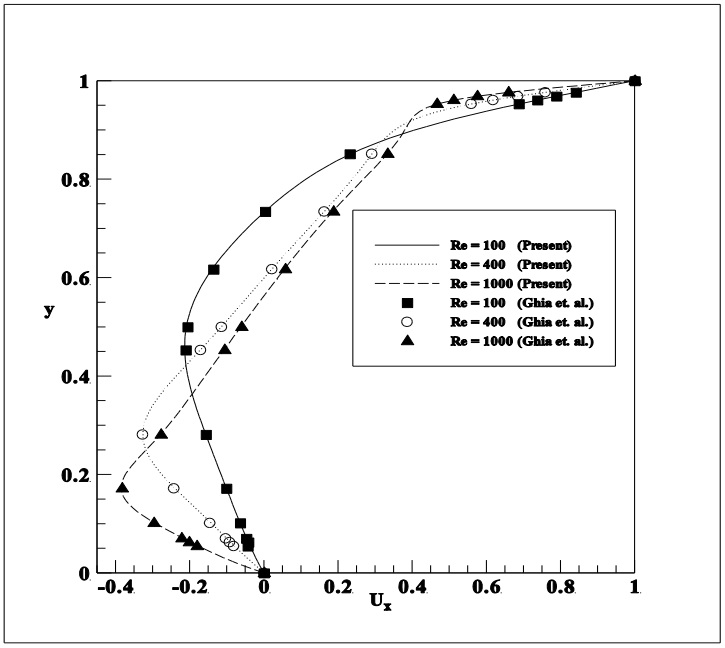

Figure 5.2: *Comparison of centerline U_x velocity*

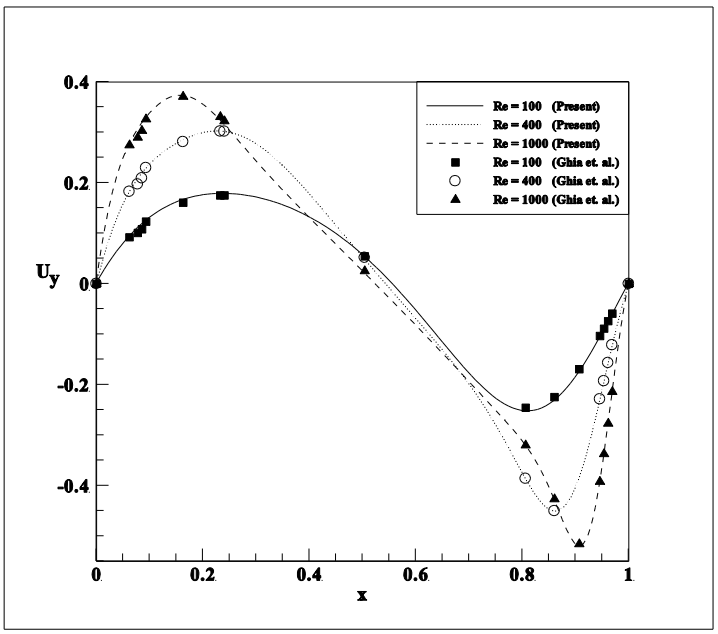

Figure 5.3: *Comparison of centerline U_y velocity*

5.2 Steady flow over semi-circular cylinder

The flow of incompressible fluids with uniform velocity U_∞ over an unconfined semi-circular cylinder. The flow schemes are shown in fig 5.4. The implemented boundary conditions are given as

The physically realistic boundary conditions for this flow are

Inlet boundary: Uniform flow and temperature condition, i.e.

$$U_x^{'} = U_\infty \;\; ; \;\; U_y^{'} = 0 \; ; \; T^{'} = T_\infty. \tag{29}$$

No-slip boundary condition at the surface of the semicircular cylinder for the flow and constant wall temperature condition for heat transfer is imposed.

$$U_x^{'} = 0 \;\; ; \;\; U_y^{'} = 0 \;\; ; \;\; T^{'} = T_w. \tag{30}$$

Outlet boundary: the outflow boundary conditions are used to model the flow at the exit where the details of the flow velocity and pressure are not known a prior it. These are appropriate where the exit flow is close to a fully developed condition.

$$\frac{\partial \emptyset}{\partial y} = 0 \tag{31}$$

where $\emptyset = U_x^{'}, \; U_y^{'}$ and $T^{'}$.

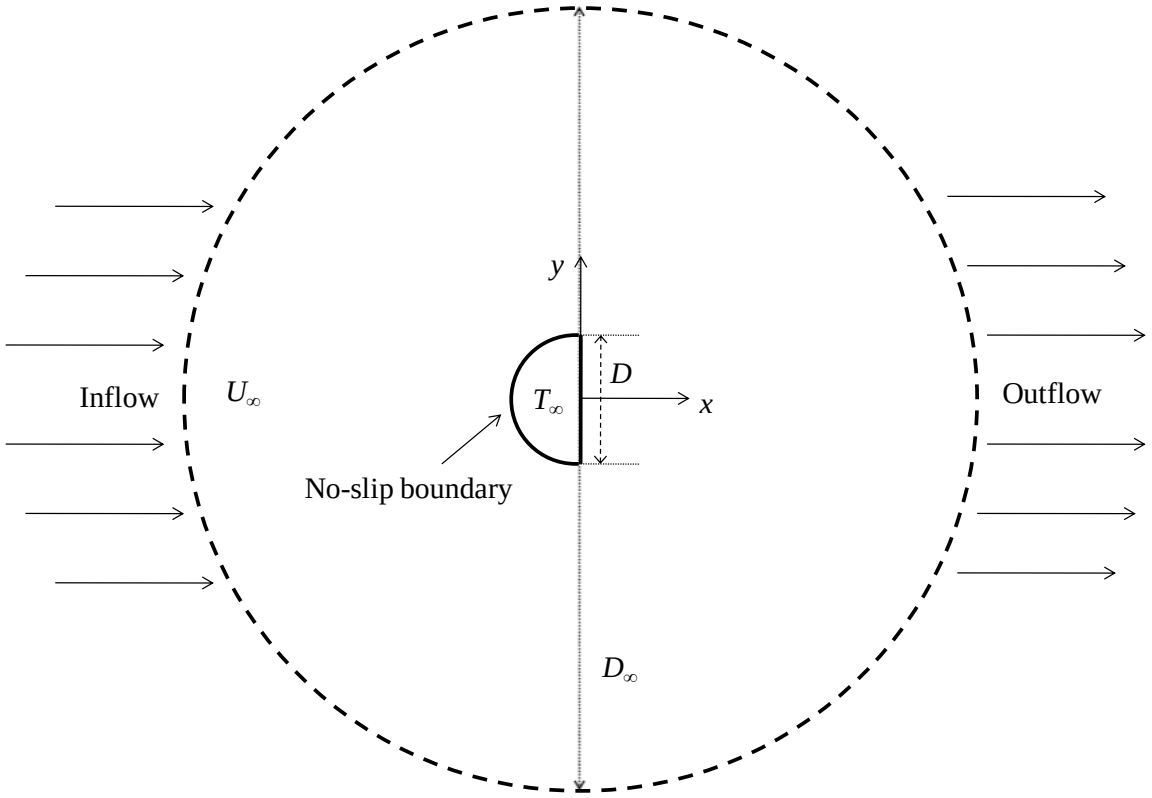

Figure 5.4: *Schematic presentation of the semi-circular cylinder*

Table 5.1: *Comparison of drag coefficients*

	Pr	***Re***	C_{DP}	C_D	Nu_{avg}
Chandra and Chabra (2010)	0.7	20	1.313	1.993	6.63427
Present	0.7	20	1.315	1.995	6.402803

The present results are almost similar to the literature values.

5.3 Forced convection heat transfer over horizontal circular cylinder within confining wall in a rectangular channel

The flow of incompressible fluids with uniform velocity U_∞ over a confined circular cylinder. The schematics of the flow are shown in figure 5.5. The results are computed and compared with *Farouk and Guceri*, 1982. The boundary conditions used here are as follows:

Inflow and Out flow boundary condition:

$$U_x^{'} = 0 \;\; ; \;\; U_y^{'} = U_\infty \;\; ; \;\; T^{'} = T_\infty. \tag{32}$$

$$\frac{\partial \emptyset}{\partial y} = 0 \tag{33}$$

where $\emptyset = U_x$, U_y and T.

No-slip boundary condition at the surface of the circular cylinder:

$$U_x^{'} = 0 \;\; ; \;\; U_y^{'} = 0 \;\; ; \;\; T = T_w \tag{34}$$

At the confined wall flow:

$$U_x^{'} = 0 \;\; ; \;\; U_y^{'} = 0 \;\; ; \;\; q^{'} = 0 \tag{35}$$

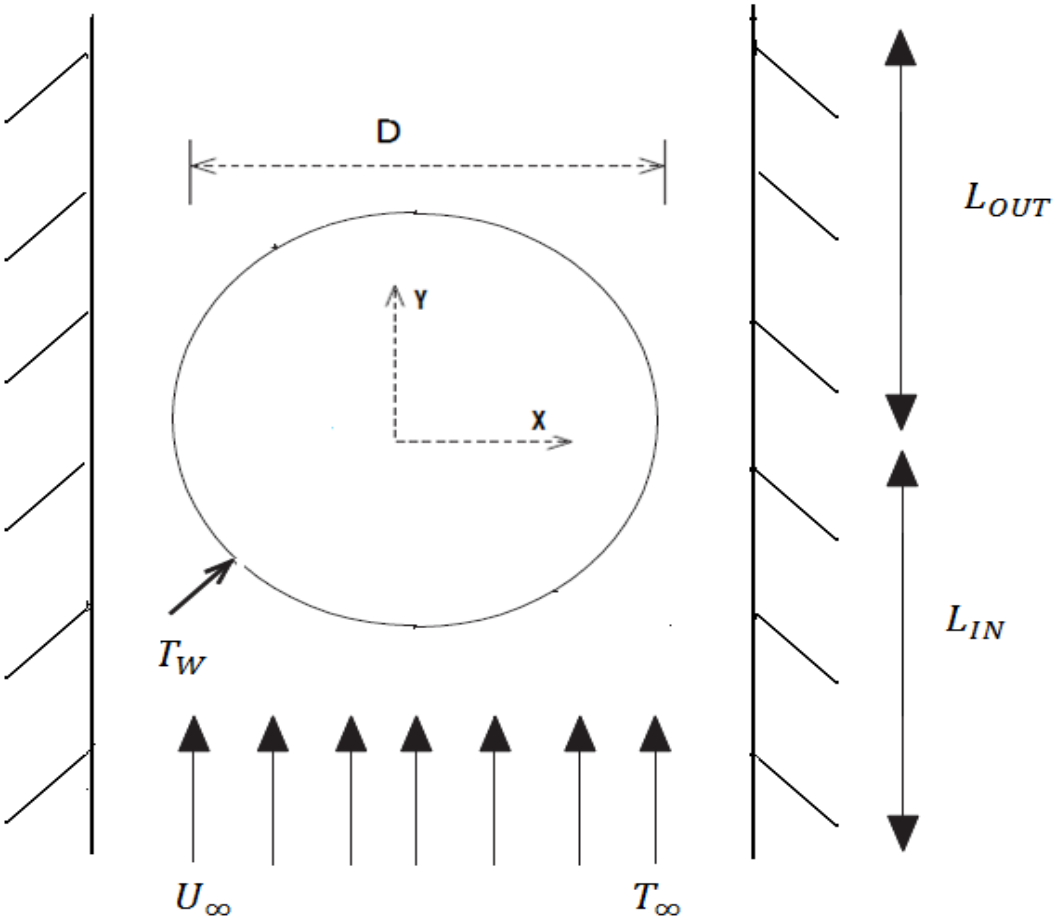

Figure5.5: *Schematic presentation of the circular cylinder within confined wall*

Table 5.2: *Comparison of results*

	Pr	***Ri***	***Re***	Nu_{avg}
Farouk and Guceri	0.7	4.12	58.01	6.63427
Present	0.7	4.12	58.01	6.402803

CHAPTER –6

Results and discussion

This chapter presents the extensive result obtained from the numerical calculations from the 2D, mixed convection and heat transfer from a semi-circular cylinder in the steady flow regime. The parameters like individual and total drag coefficients and Nusselt number have been studied to delineate their dependence on dimensionless parameters such as Reynolds number and Prandtl number for the semi-circular cylinder. The detailed kinematics of the flow and heat transfer characteristics have been visualized in terms of stream lines and temperature contours. The flow and heat transfer fields are obtained by the variation of Nusselt number, average Nusselt number, individual and total drags coefficients over the surface of the semi-circular cylinder. In this study, investigation has been carried out when imposed flow and gravity induced flow are in the upward direction (aiding buoyancy) for the semi-circular cylinder placed in a channel.

6.1 Fluid flow characteristics

6.1.1 Streamline patterns

Figs 6.1 and 6.2 in the left half presents the flow patterns around the semi-circular cylinder in terms of stream line profiles for combination of Reynolds number, Richardson number at Prandtl number (Pr =0.7, 50). The trends can be summarized as follow:

No separation is seen for the Reynolds number (Re=1) at Pr = 0.7 for all values of Ri. For constant Ri, the separation bubble increases in size whereas at constant Re, bubble shrinks with increase in Ri. The effect of buoyancy- induced flow is seen to suppress the size of the wake. The size of the wake region decreases with the increasing value of the Richardson number or the Prandtl number or both. At lower value of Reynolds, buoyancy induced current contributes to the strength of the flow and leading towards the crowding of the streamlines at the front surface of the semi-circular cylinder.

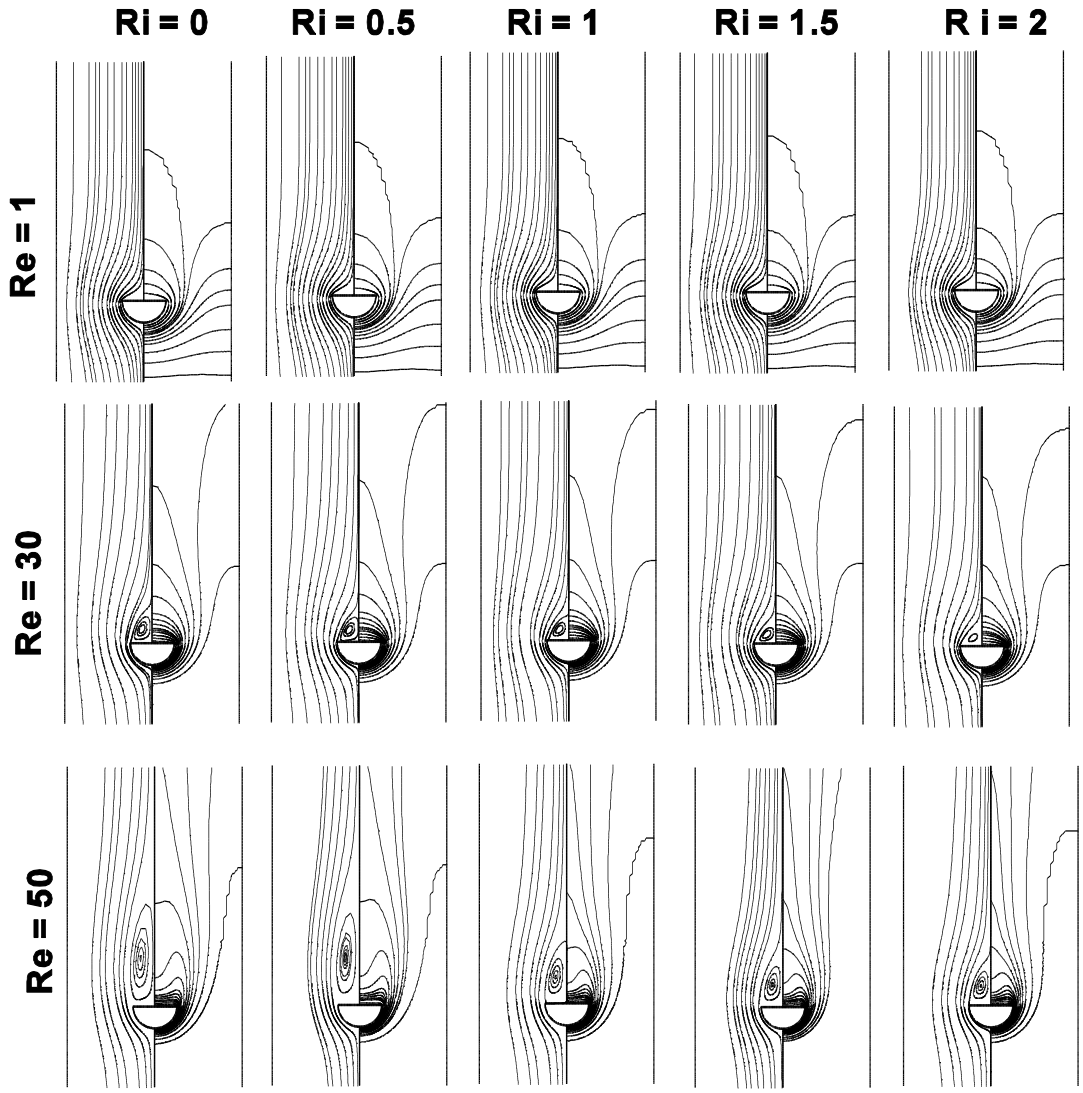

Fig 6.1: *Streamline patterns (left half of the figure) and isotherms (right half of the figure)* $Pr = 0.7$

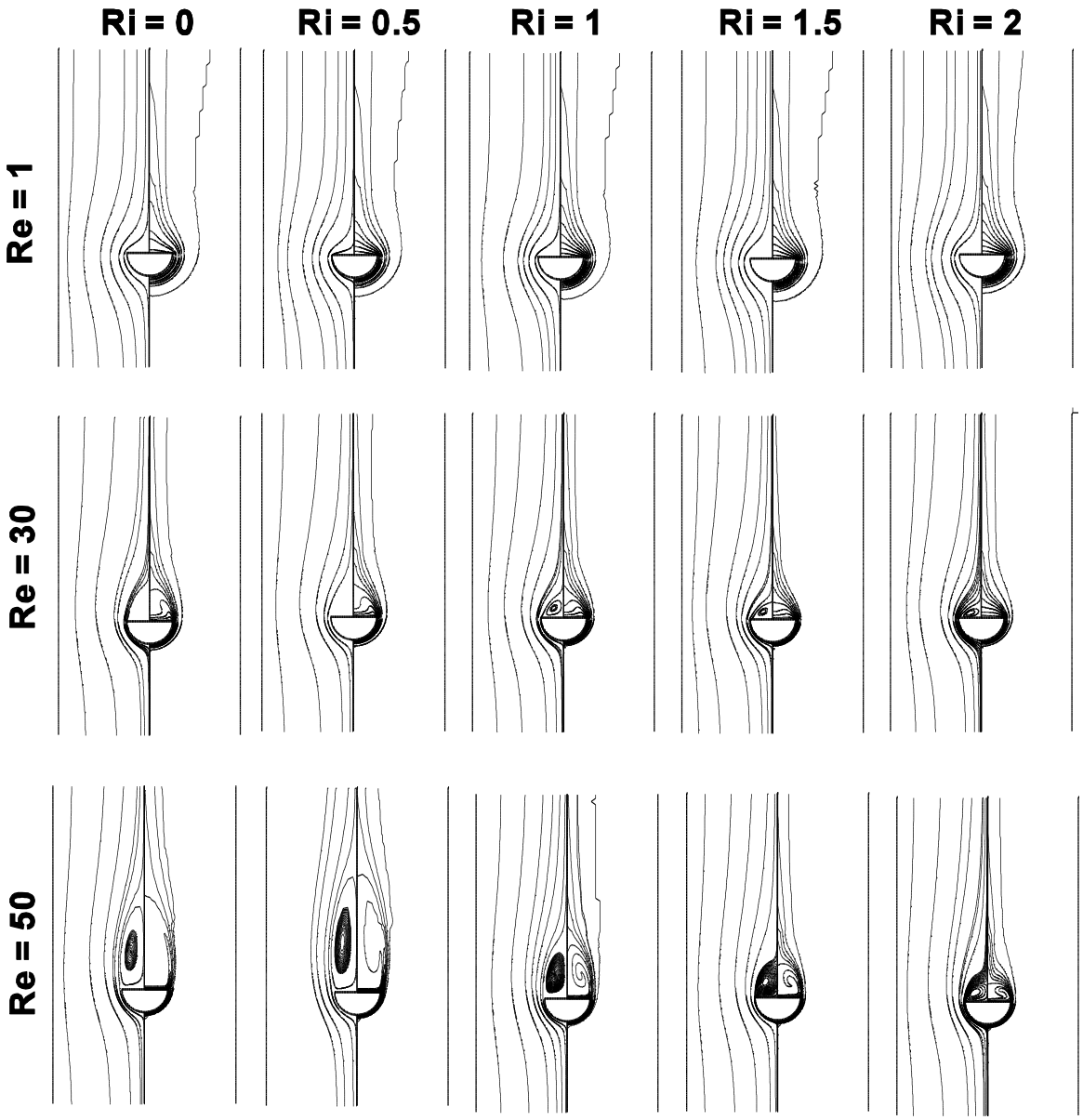

Fig 6.2: *Streamline patterns (left half of the figure) and isotherms (right half of the figure)*

Pr = 50

6.1.2 Pressure coefficients

The distribution of the pressure coefficient, C_P on the surface of the semi-circular cylinder are shown fig 6.3 for various combinations of the Reynolds number, Richardson number and Prandtl number. At the low value of Reynolds number (Re=1) the value of C_P decreases along the body contour, reaching its minimum value at point B followed by a very little recovery between point B and point C. This indicates that the pressure drag contributes significantly to the overall drag even at such low Reynolds numbers. At high value of Reynolds number (Re=50), the maximum value of C_p found at front stagnation and lowest value remains at point B. The similar trend is seen for high value of *Re* and *Pr* (Re=50, Pr = 50) .The value of the C_P decreases at the corner point B with increasing value of *Ri*. The decrease in the value of pressure coefficient is observed in between point A and point B instead of the sudden drop at point B.

6.1.3 Drag coefficients

The Drag value (C_{DP} and C_D) are presented in fig 6.4 for the ranges of the *Re*, *Pr* and *Ri*. The value of C_{DP} and C_D suddenly decreases as the value of Re changes from 1 to 10. This behave is due to the boundary layer separation behind the semi-circular cylinder. The stream line profile also shows that the flow is attached to the body contours and at Re = 10 it get separated and separate bubble form. The size of the bubble increases with increase in the value of *Re*. Hence, the sudden drop in the drag values is seen between Re = 1 to Re = 10.At low *Re*, the influence of buoyancy (*Ri*) is almost negligible. The influence of *Ri* increases with increase in the value of *Re* and *Pr*. The drag increases with increase in *Pr*.

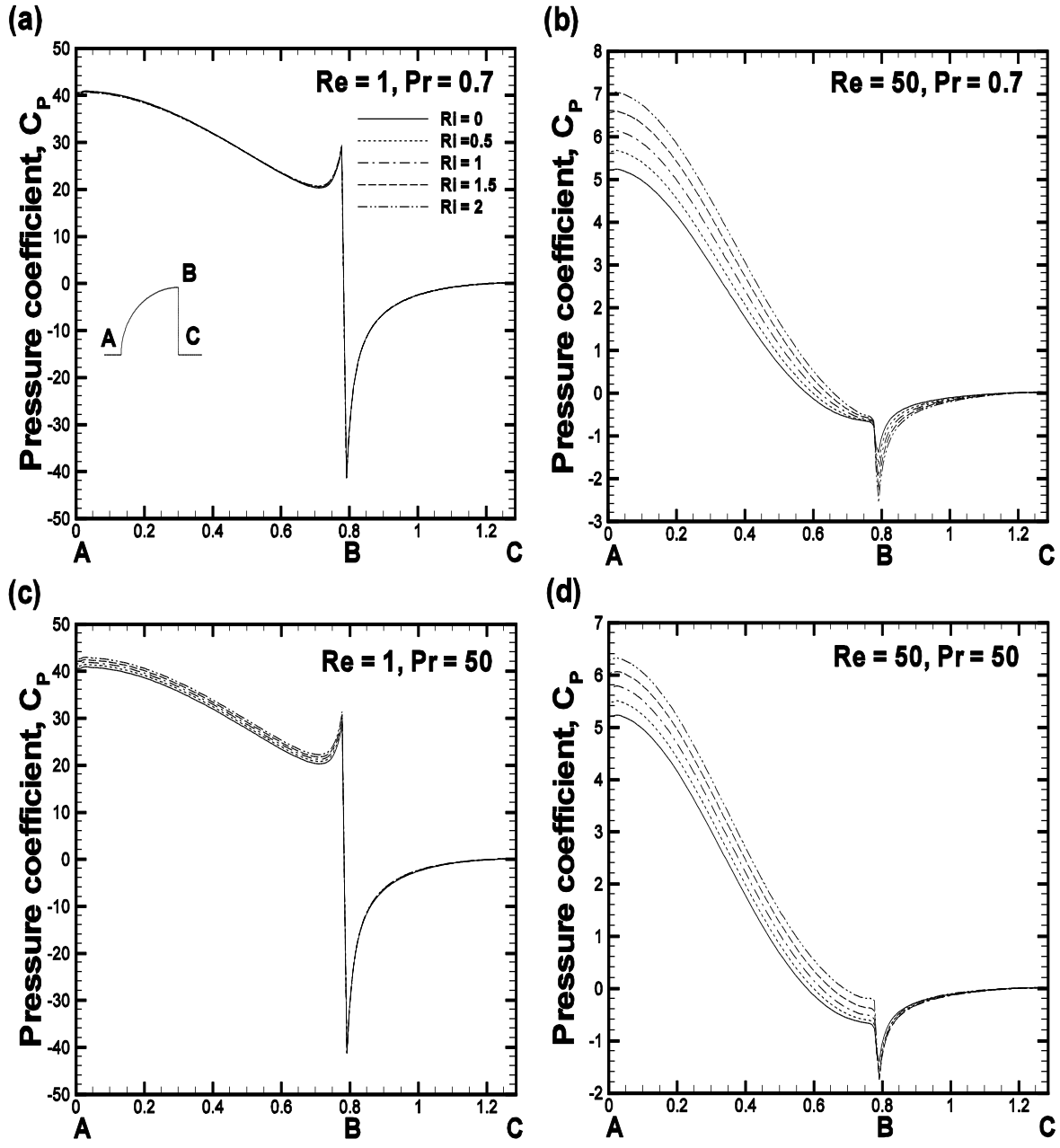

Fig 6.3: *Distribution of pressure coefficient along the surface of semi-circular cylinder*

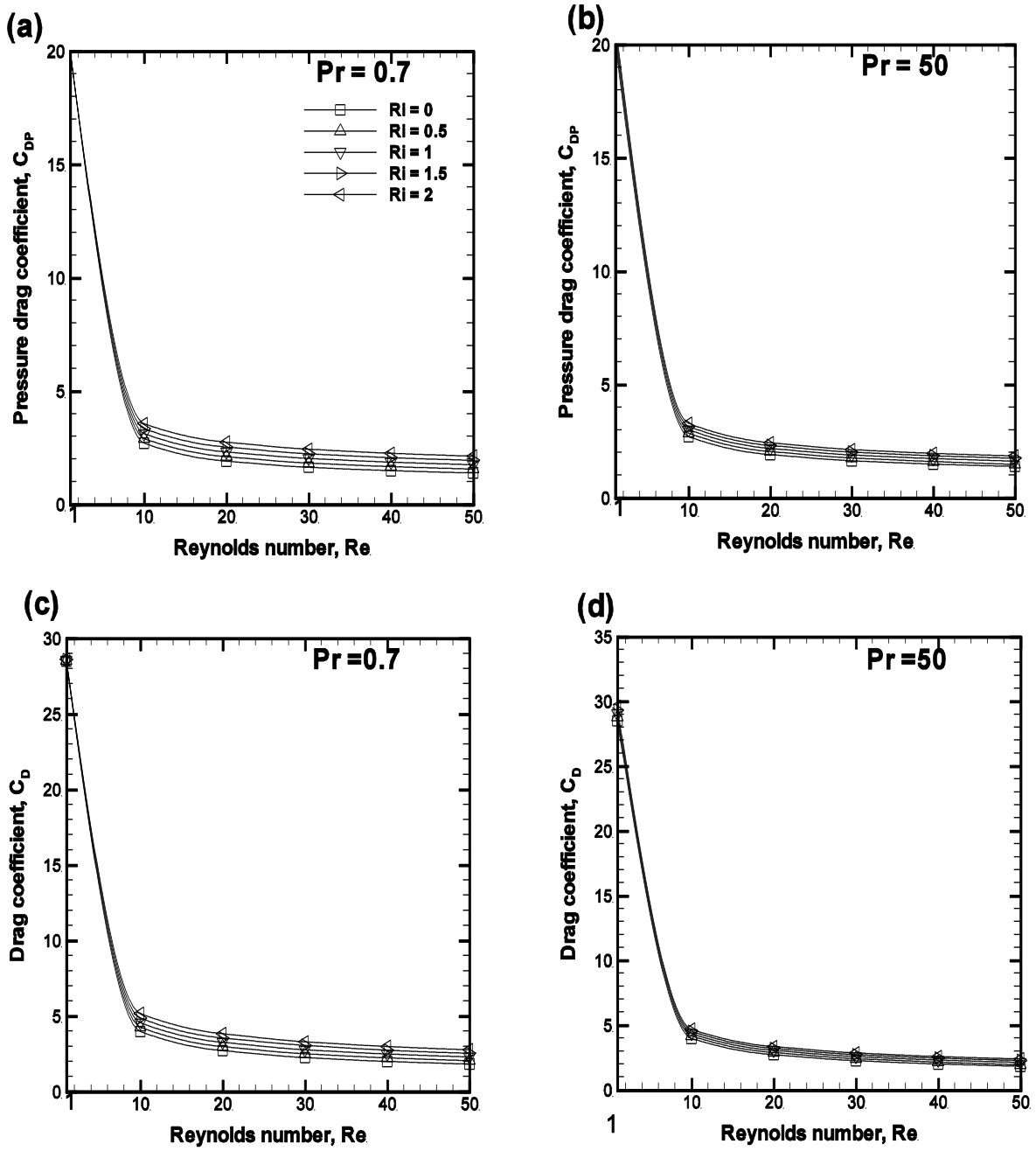

Fig 6.4: *Distribution of drag coefficient along the surface of semi-circular cylinder*

6.2 Heat transfer

6.2.1 Isotherm patterns

Isotherm contours are shown in the right half of fig 6.1 - 6.2. The isotherm contours are qualitatively similar to the streamline patterns shown in the left half. The crowding of isotherms increases on the front surface of the semi-circular cylinder with increasing *Re* and *Pr.* The crowding of isotherms on the curved surface presents higher *Nu* here than that on the flat surface. This shows that curved surface transfer much more heat than the rear plane surface of semi-circular cylinder.

6.2.2 Local Nusselt number

The variation of local Nusselt number along the surface of the semi-circular cylinder as shown in fig 6.5. Under all conditions, the rear surface contributes very little to the overall heat transfer. This is not surprising because the temperature gradient is a maximum at the front stagnation point and it progressively decreases along the curved surface of the cylinder. At point B, Nusselt number shows its maximum value and it decreases along the rear surface of the cylinder. This is due to the presence of sharp corner at point B and the sudden boundary of isotherm profile heat transfer on heat. Again, the influence of *Ri* increases with increase in *Re* at constant *Pr.* At constant *Pr* and *Re*, the value of local *Nu* increases with increase in *Ri* at front curved surface whereas in the rear it decreases with increase in *Ri*. At *Re* = 50, *Pr* = 0.7, the influence of *Ri* at front surface is more prominent than rear surface, whereas at *Re* = 50, *Pr* = 50, the influence of *Ri* increases in the rear of the semi-circular cylinder. This is due to the complex inter-planer between the field parameter *Re, Pr* and *Ri*.

6.2.3 Average Nusselt number

It is frequently needed to estimate the value of the average heat transfer coefficient in a new application, i.e., for known value of *Re, Ri,* and *Pr*. The functional dependence of the average Nusselt number on the Reynolds number (*Re*), Prandtl number (*Pr*) and Richardson number (*Ri*) is shown in the fig 6.6. The average Nusselt number shows positive dependence with the Reynolds number, Prandtl number and Richardson number. At low Prandtl numbers, the effect of Richardson number is seen to be quite distinct; it progressively diminishes with the

increasing value of *Pr* up to 7. Further, increase in the value of *Pr* presents increase in the value of the *Ri* (fig 6.6). Hence, Nu_{avg} shows complex dependence on *Ri* in case of mixed convection heat transfer. Overall, Nu_{avg} increase with increase in *Re* and *Pr*. The rate of heat transfer increases with increase in the Prandtl number.

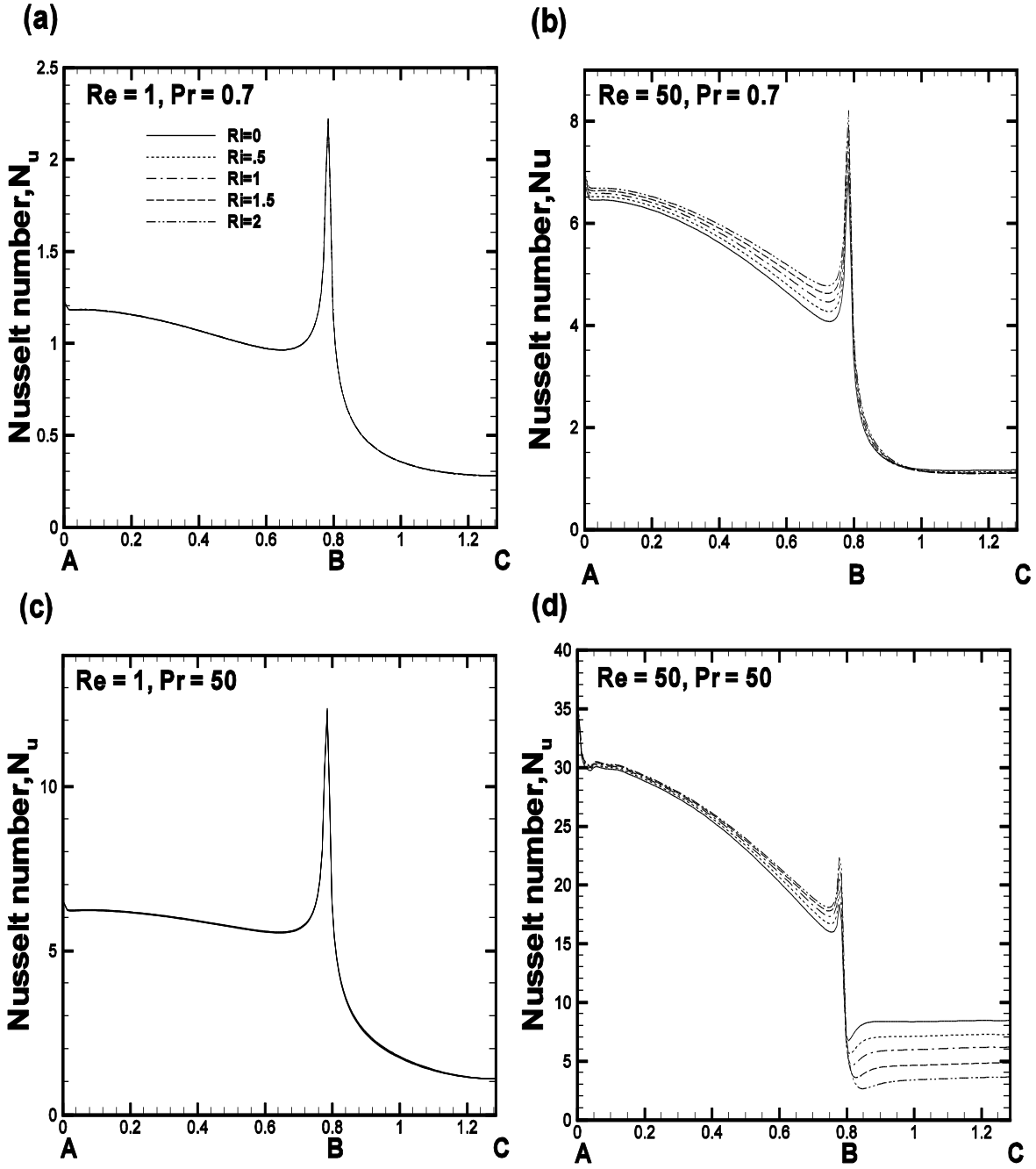

Fig 6.5: *Distribution of Nusselt number along the surface of semi-circular cylinder*

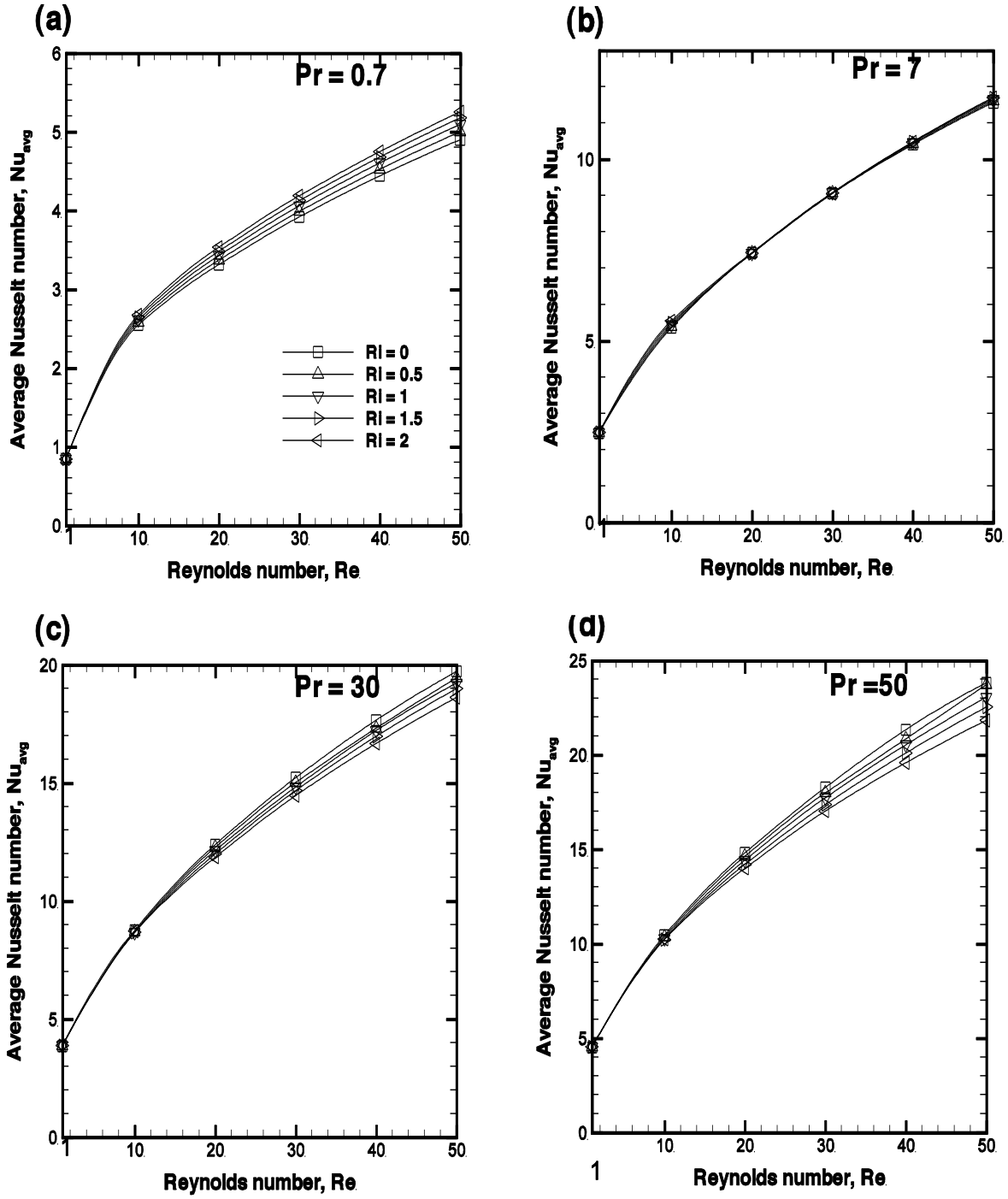

Fig 6.6: *Distribution of average Nusselt number along the surface of semi-circular cylinder*

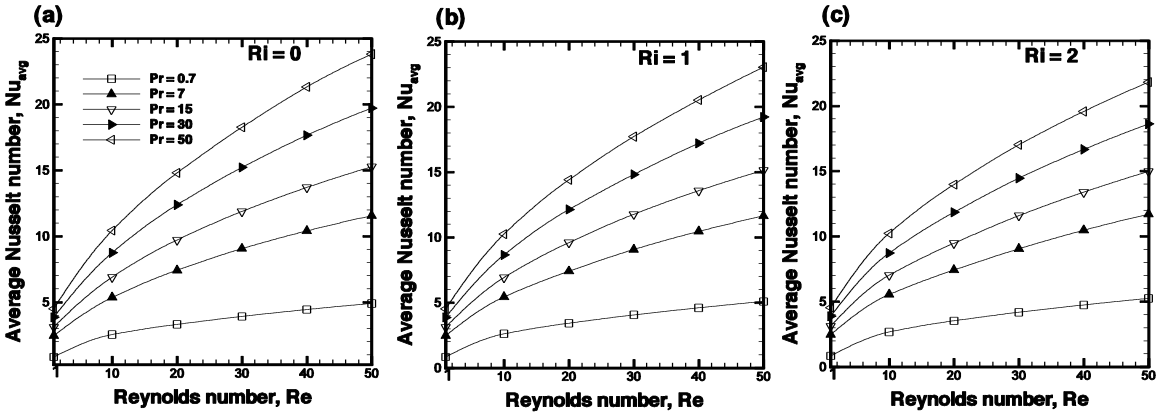

Fig 6.7: *Distribution of average Nusselt number along the surface of semi-circular cylinder*

In fig 6.7, as the value of *Ri* increases from 0 to 2. The value of Nu_{avg} is almost constant and having little influence at *Re* = 50.

Table 6.1: *Dependence of C_D on Re, Ri and Pr.*

Re	***Pr* = 0.7**					***Pr* = 30**				
	***Ri*=0**	***Ri*=0.5**	***Ri*=1**	***Ri*=1.5**	***Ri*=2**	***Ri*=0**	***Ri*=0.5**	***Ri*=1**	***Ri*=1.5**	***Ri*=2**
1	28.47	28.51	28.53	28.57	28.60	28.47	28.79	29.12	29.41	29.72
10	3.96	4.25	4.55	4.85	5.160	3.96	4.16	4.36	4.54	4.71
20	2.69	2.96	3.24	3.53	3.81	2.69	2.87	3.05	3.21	3.36
30	2.23	2.49	2.75	3.95	3.28	2.24	2.41	2.57	2.73	2.87
40	1.98	2.21	2.47	2.72	2.97	1.98	2.14	2.31	2.46	2.59
50	1.81	2.03	2.28	2.52	2.75	1.81	1.95	2.12	2.27	2.40
	***Pr* = 7**					***Pr* = 50**				
1	28.47	28.81	29.20	29.56	29.91	28.47	28.76	29.03	29.31	29.59
10	3.96	4.2	4.45	4.68	4.92	3.96	4.15	4.33	4.51	4.66
20	2.69	2.90	3.11	3.32	3.51	2.69	2.86	3.03	3.18	3.32
30	2.23	2.43	2.62	2.81	2.99	2.23	2.39	2.55	2.70	2.83
40	1.98	2.16	2.35	2.53	2.71	1.98	2.12	2.28	2.43	2.55
50	1.81	1.98	2.17	2.35	2.51	1.81	1.92	2.10	2.25	2.37

CHAPTER –7

Conclusions and future recommendations

Conclusions

This chapter summarizes the key finding of the present work regarding the mixed convection heat transfer from a confined semi-circular cylinder for the following range of the conditions: $0.7 \leq Pr \leq 50$, $1 \leq Re \leq 50$, $0 \leq Ri \leq 50$ and $\beta = 4$.

The detailed flow and thermal field have been explored in terms of stream lines and isotherm profiles. The distributions of pressure coefficient and local Nusselt number along the surface of the semi-circular cylinder have been presented. The overall gross behaviour is interpreted in terms of the individual and total drag coefficients and average Nusselt number. The wake region is small at lower value of Reynolds number *i*n the rear of the semi-circular cylinder which disappears with the increasing values of the Prandtl number and the Richardson number and the flow remains attached to the surface of the semi- circular cylinder. The value of the pressure coefficient is found to be maximum at the front stagnation point and at low value of Reynolds number the value of C_P decreases along the body contour, reaching its minimum value at point B. The drag coefficients decrease with increase in the Reynolds number. The rear surface contributes very little to the overall heat transfer and local Nusselt number is found to maximum at corner point (B) of the semi-circular. Overall, the average Nusselt number shows positive dependence with the Reynolds number, Prandtl number and Richardson number.

Future recommendations

The following suggestions can be made for the future work in this field:

- This work can be further extended for the 2*D* unsteady flow regime.
- The identification of parameters for the flow transition from 2*D* to 3*D*.
- In the present work the mixed convection problem is investigated for the aiding buoyancy flow of Newtonian fluid and it can be extended to the non – Newtonian fluid.

References

Abbassi, H.S., Turki and Nasrallah, S.N. (2001). "Numerical investigation of forced convection in a plane channel with a built-in triangular prism", "*International Journal of Thermal Sciences*, 40: 649-658.

Anuar, I. (2009). "Mixed convection boundary layer flow over a vertical cylinder with prescribed surface heat flux", *School of Mathematical Sciences*, Universiti Kebangsaan Malaysia, 43600 UKM Bangi, Selangor, Malaysia. J. Phys. A : Math. Theor, 42 (2009) 195501.

Bharti, R.P., Sivakumar, P. and Chhabra R.P. (2008). "Forced convection heat transfer from an elliptical cylinder to power-law fluids", *International Journal of Heat and Mass Transfer*, 51: 1838-1853.

Boisaubert, N. and Texier, A. (1998). "Effect of splitter plate on the near-wake development of a semi-circular cylinder", *Experimental Thermal and Fluid Science*, 16, 100-111.

Boisaubert, N., Coutanceau, M. and Ehrmann, P. (1996). "Comparative early development of wake vortices behind a short semicircular-section cylinder in two opposite arrangements", *Journal of Fluid Mechanics*, 327, 73-99.

Boisaubert, N., Coutanceau, M. and Texier, A. (1997). "Manipulation of the starting semicircular cylinder near-wake by means of a splitter plate", *Journal of Flow Visualization and Image Processing*, 4, 211-221.

Chandra and Chhabra (2011). "Momentum and heat transfer characteristics of a semi-circular cylinder immersed in power-law fluids in the steady flow regime", *International Journal of Heat and Mass Transfer*, 54, 2734–2750.

Chandra and Chhabra (2011). "Momentum and heat transfer characteristics of a semi-circular cylinder immersed in unconfined flowing Newtonian fluid", *International Journal of Heat and Mass Transfer* 54, 225–241.

Chatterjee, D. and Amiroudine, S. (2009). "Two-dimensional mixed convection heat transfer from confined tandem square cylinders in cross-flow at low Reynolds numbers" LPMI, Arts et Métiers Paris Tech, 2 Boulevard du Ronceray, BP 93525, 49035 Angers, Cedex 01, France. *International Communications in Heat and Mass Transfer.* 37 (2010) 7–16.

Coutanceau, M., Migeon, C. and Ehrmann, P. (2000). "Particulars of the cross and span-wise near-wake development of a short semi-circular shell through the transition Re-range ($60 \leq Re \leq 600$)", *Journal of Visualization* 3(1), 9-26.

Dhiman, A.K., Anjaiah, N., Chhabra, R.P. and Eswaran, V. (2007). "Mixed convection from a heated square cylinder to Newtonian and power-law fluids", *Journal of Fluids Engineering*, 129: 506-513.

Dhiman, A.K., Chhabra, R.P. and Eswaran, V. (2007). "Steady mixed convection across a confined square cylinder", *International Communications in Heat and Mass Transfer*, 35: 47-55.

Dhole, S.D., Chhabra, R.P. and Eswaran, V. (2006). "Forced Convection Heat Transfer from a Sphere to Non-Newtonian Power Law Fluids", *American Institute of Chemical Engineers* Vol. 52, No. 11 DOI 10.1002/aic 3659.

Ghia, U., Ghia, K.N. and Shin, C.T. (1982). "High-Re solutions for incompressible flow using the Navier- Stokes equations and multi grid method", *Journal of Computational Physics*, 48: 387- 411.

Hocking, G.C. and Vanden-Broeck, J.M. (2008). "The effect of gravity on flow past a semi-circular cylinder with a constant pressure wake", *Applied Mathematical Modeling* 32, 677-687.

Karniadakis, G.E. and Brown, G.L. (1995). "Vorticity transport in modelling three dimensional unsteady shear flows", *Physics of Fluids*, 7: 688-690.

Kiya, M. and Arie, M. (1975). "Viscous shear flow past small bluff bodies attached to a plane wall *Journal of Fluid Mechanics"*, 69(4), 803-823.

Kumarasamy, S. and Barlow, J.B. (1995). "Interference of plane wall on periodic shedding behind a half cylinder", *26th AIAA Fluid Dynamics Conference*, San Diego, CA, American Institute of Aeronautics and Astronautics, AIAA 95-2285: 1-8.

Nada, S.A. and Mowad, M. (2003). "Free convection from a vertical and inclined semi-circular cylinder at different orientations", *Alexandria Engineering Journal*, 42: 273-283.

Nada, S.A., El-Batsh, H. and Moawed, M. (2007). "Heat transfer and fluid flow around semi-circular tube in cross flow at different orientations", *Heat Mass transfer* 43, 1157-1169.

Rahul, C.P., Bharti, R.P. and Chhabra, R.P. (2008). "Forced Convection Heat Transfer in Power Law Liquids from a Pair of Cylinders in Tandem Arrangement", *Ind. Eng. Chem. Res.* 2008**,** *47*, 9141–9164.

Sahu, A.K., Chhabra, R.P. and Eswaran, V. (2009). "Forced convection heat transfer from a heated square cylinder to power-law fluids in the unsteady flow regime", *Numerical Heat Transfer*, Part A, 56: 109-131.

Sanitjai .S. and Goldstein, R.J. (2003)." Department of Mechanical Engineering, University of Minnesota, Heat Transfer Laboratory, 125, Mechanical Eng. Building,111 Church Street SE, Minneapolis, MN 55455", USA. *International Journal of Heat and Mass Transfer* 47 (2004) 4795–4805.

Soares, A. A., Ferreria, J.M. and Chhabra, R.P. (2005). "Flow and forced convection heat transfer in cross flow of non-Newtonian fluids over a circular cylinder", *Industrial and Engineering Chemistry Research*, 44: 5815-5827.

Soares, A.A., Anacleto, J., Caramelo, L., Ferreira, J.M. and Chhabra, R.P. (2009). "Mixed convection from a circular cylinder to power-law fluids", *Industrial and Engineering Chemistry Research*, 48: 8219–8231.

Sophy, H., Sada and Bouard, D. (2002). "Calcul de I'ecoulement autour d'un cylindre semi-circulaire par une method de collocation", *C R Mecanique*, 330.

Srinivas, Bharti, R.P. and Chhabra, R.P. (2009). "Mixed convection heat transfer from a cylinder in power-law fluids: Effect of aiding buoyancy." *Industrial and Engineering Chemistry Research*, 48: 9735–9754**.**